Supplementary Information

Interfacial Charge Redistribution in Hollow Fe_3C/MoN Heterostructures Promotes Bifunctional Electrocatalysis for Alkaline Zinc-Air Batteries

Tailin Ji,† Xinyu Yang,† and Xinxin Xu*

Department of Chemistry, College of Sciences, Northeastern University, Shenyang 110819, Liaoning, China. Email: xuxx@mail.neu.edu.cn

† These authors contributed equally to this work.

Materials

Fumaric acid ($C_4H_4O_4$, 99%, AR), iron(III) nitrate nonahydrate ($Fe(NO_3)_3 \cdot 9H_2O$, 99%, AR), dicyandiamide (DCDA, $C_2H_4N_4$, 99%, AR), nickel(II) chloride hexahydrate ($NiCl_2 \cdot 6H_2O$, 99%, AR), ammonium molybdate ($(NH_4)_6Mo_7O_{24} \cdot 4H_2O$, 99%, AR), Zinc acetate dihydrate ($Zn(Ac)_2 \cdot 2H_2O$, 99%, AR), potassium hydroxide (KOH, 99%, AR), N,N′-methylenebisacrylamide (MBAA, 99%, AR), potassium persulfate ($K_2S_2O_8$, 99%, AR), ammonia solution ($NH_3 \cdot H_2O$, AR), and acrylic acid (AA, $C_3H_4O_2$, AR) were purchased from Beijing Innochem Science & Technology Co., Ltd. All the chemicals were used as received without further purification. All standard solutions were prepared with Milli-Q water with a resistivity of 18 MΩ·cm.

The synthesis of MIL-88A

MIL-88A was synthesized via a hydrothermal method. Typically, 139 mg of fumaric acid was dissolved in 25 mL of deionized water at 70°C under stirring for 10 min to form a clear solution. Subsequently, 525 mg of $Fe(NO_3)_3 \cdot 9H_2O$ was added, and the mixture was continuously stirred for another 10 min. The resulting homogeneous solution was then transferred into a Teflon-lined stainless-steel autoclave and maintained at 110°C for 6 h. After naturally cooling to room temperature, the obtained precipitate was collected by centrifugation, thoroughly washed with deionized water and absolute ethanol several times to remove residual reactants, and finally dried in an oven at 80°C to obtain MIL-88A.

The synthesis of $NiMo_6$ polyoxometalate

Nickel-containing Anderson-type polyoxometalate ($NiMo_6$) was synthesized via a facile coprecipitation method at ambient conditions. Typically, an aqueous solution of $(NH_4)_6Mo_7O_{24} \cdot 4H_2O$ was first prepared and used as the molybdenum source. Subsequently, $NiCl_2 \cdot 6H_2O$ was dissolved in deionized water and added dropwise into

the above solution under continuous stirring, maintaining a Mo: Ni molar ratio of 6:1. After complete mixing, dilute ammonia solution was introduced to adjust the pH of the system to 5–6, where the Anderson-type structure is thermodynamically favored. Under this mildly acidic to near-neutral condition, a coprecipitation process occurred, leading to the formation of the target $NiMo_6$ polyoxometalate ammonium salt. The resulting precipitate was collected by filtration, thoroughly washed with deionized water to remove residual ions, and finally dried at room temperature to obtain the final product.

The synthesis of hollow Mo@MIL-88A intermediate

The hollow Mo@MIL-88A intermediate was prepared via a $NiMo_6$-assisted etching process. Typically, 100 mg of MIL-88A and 100 mg of $NiMo_6$ were dispersed in 30 mL of deionized water under stirring for 30 min. The resulting suspension was then transferred into a 50 mL Teflon-lined stainless-steel autoclave and heated at 120°C for 1 h. After cooling naturally to room temperature, the product was collected by centrifugation, washed several times with deionized water and absolute ethanol, and dried in an oven at 80°C for further use.

The synthesis of Fe_3C/MoN

The Mo@MIL-88A intermediate and DCDA were thoroughly ground in an agate mortar at a mass ratio of 1:20 to obtain a homogeneous mixture. The resulting powder was then placed in a tubular furnace and annealed at 800°C for 2 h under a N_2 atmosphere. After cooling to room temperature under N_2 protection, the final black powder was collected and denoted as **Fe_3C/MoN**. For comparison, Fe_3C and MoN were prepared by calcining MIL-88A and $NiMo_6$, respectively, under the same conditions.

Preparation of PAAK Gel Polymer Electrolyte

1 g of poly(vinyl alcohol) (PVA) was dissolved in 20 mL of ultrapure water under stirring at 90˚C for 2 h to obtain a homogeneous solution. After cooling to 60˚C, 11 mL of 8.4 M potassium hydroxide solution, 0.025 g of N,N'-methylenebisacrylamide, and 10.08 g of acrylic acid were added, followed by stirring for 30 min at 60˚C. Then 5 mL of 0.15 M potassium persulfate solution was added, followed by vigorous stirring for about 20 seconds. The resulting mixture was poured into a Petri dish to form a gel with a thickness of approximately 2–4 mm and dried at 60˚C for 3 h. Finally, the obtained gel was immersed in a 6 M KOH + 0.2 M $Zn(Ac)_2$ solution for 24 h to obtain the PAAK gel polymer electrolyte.

Characterizations

XRD patterns were recorded using a Philips X'Pert Pro Super X-ray diffractometer with Cu Kα (λ = 1.5418 Å) radiation. XPS measurements were performed using Mg Kα radiation (1253.6 eV) as the excitation source (ESCALAB 250Xi, Thermo Fisher Scientific). UPS (PHI5000 VersaProbe III) was used to determine the work function. The bandgap of the sample was analyzed by UV-vis DRS (Shimadzu, UV-3600Plus). Morphology of the samples was observed using SEM (ultra plus, ZEISS) and TEM (JEOL, JEM-2100F). N_2 adsorption-desorption measurements were performed on a Micromeritics ASAP 2460 instrument at 77 K.

DFT Calculations

DFT calculations were performed using the Vienna *ab initio* simulation package (VASP) within the generalized gradient approximation (GGA) and the Perdew–Burke–Ernzerhof (PBE) functional. The projector augmented wave (PAW) method was used, with a plane-wave cutoff energy of 500 eV. The electronic convergence criterion was set to 10^{-5} eV, and the structures were relaxed until the forces on each

atom were below 0.05 eV $Å^{-1}$. Grimme's DFT-D3 method was used to account for dispersion interactions. A vacuum layer of 20 Å and a 2 × 2 × 1 Monkhorst–Pack k-point grid were adopted. Based on these calculations, the optimized structures of Fe_3C, MoN, and **Fe_3C/MoN** were obtained, and the corresponding DOS was calculated with the Fermi level set to 0 eV.

Electrochemical Measurements

Electrochemical measurements were conducted using a CHI-760E electrochemical workstation (Chenhua, Shanghai). For all electrochemical evaluations, including ORR, OER, ZAB, and FZAB tests, the commercial benchmark catalysts (Pt/C, RuO_2, or their mixture) were tested under identical conditions to **Fe_3C/MoN**, namely the same ink formulation, catalyst loading, electrode preparation procedure, and testing parameters.

RRDE test in ORR

RRDE tests were conducted in an O_2-saturated 0.1 M KOH electrolyte using a three-electrode system. Working electrode was fabricated as follows: the mixture of **Fe_3C/MoN** (2 mg) and conductive carbon black (Vulcan XC-72R, 8 mg) was dispersed in aqueous solution of water (0.8 mL), ethanol (0.15 mL) and 50 μL Nafion (5 %). The ink (10 μL) was dropped on RRDE (electrode area is 0.2475 cm^2) and served as working electrode. Graphite electrode and Ag/AgCl electrode (3 M KCl) were employed as counter and reference electrodes. The disk potential was cycled from 0 to 1.0 V (vs. RHE) with a rotation rate of 10 $mV \cdot s^{-1}$. The ring potential was constant at 1.2 V (vs. RHE). The H_2O_2 selectivity (H_2O_2%) and electron transfer number (n) were calculated with Eq. 1 and 2. In these equations, I_D and I_R represent disk and ring currents density. N (N = 0.37, obtained from $K_3Fe(CN)_6$ reduction experiments at various rotation rates) is the current collection efficiency of the Pt ring.

$$H_2O_2\% = (200 \times I_R/N)/(I_R/N + I_D) \quad (1)$$

$$n = 4 \times I_d/(I_R/N + I_D) \quad (2)$$

RDE test in ORR

RDE tests were also conducted in an O_2-saturated 0.1 M KOH electrolyte using a three-electrode system, in which Graphite electrode and Ag/AgCl electrode (3 M KCl) were employed as counter and reference electrodes. Working electrode was fabricated as follows: the mixture of **Fe_3C/MoN** (2 mg) and carbon black (8 mg) was dispersed in aqueous solution of water (0.8 mL), ethanol (0.15 mL) and 50 μL Nafion (5 %). The ink (10 μL) was dropped on RDE (electrode area is 0.196 cm^2) and served as working electrode. Linear sweep voltammetry (LSV) was recorded at 10 $mV \cdot s^{-1}$. The rotating rates of RDE were 400, 625, 900, 122, 1600, 2025 and 2500 rpm. The electron transfer number was calculated by using the Koutechy-Levich (K-L) equation (Eq. 3). In this equation, j is the measured current density, j_k is the kinetic current density, ω is the electrode rotating rate. The parameter B could be calculated from the slope of the K-L plots based on the following Levich equation (Eq. 4), in which n is the electron transfer number per oxygen molecule, F is the Faraday constant (F= 96485 $C \cdot mol^{-1}$), D_0 is the diffusion coefficient of O_2 in 0.1 M KOH ($D_0 = 1.9 \times 10^{-5}$ $cm^2 \cdot s^{-1}$), v is the kinetic viscosity ($v = 0.01$ $cm^2 \cdot s^{-1}$) and C_0 is the bulk concentration of O_2 ($C_0 = 1.2 \times 10^{-6}$ $mol \cdot cm^{-3}$).

$$1/j = 1/j_k + 1/B\omega^{1/2} \quad (3)$$

$$B = 0.62nF(D_0)^{2/3}(V)^{-1/6}C_0 \quad (4)$$

OER test

OER was conducted in a N_2-saturated 1 M KOH electrolyte. Three-electrode system was employed. Working electrode was fabricated as follows: the mixture of **Fe_3C/MoN** (2 mg) and carbon black (8 mg) was dispersed in aqueous solution of

water (0.8 mL), ethanol (0.15 mL) and 50 μL Nafion (5 %). The ink (10 μL) was dropped on glassy carbon (GC) electrode (electrode area is 0.196 cm^2). Graphite electrode and Ag/AgCl electrode (3 M KCl) were employed as counter and reference electrodes.

EIS and multi-cycle CV tests

Electrochemical impedance spectroscopy (EIS) measurements were conducted over a frequency range of 0.01 to 100k Hz. The electrochemically active surface area (ECSA) was determined by measuring the C_{dl} within a small potential range, with rotation rates of 10, 20, 30, 40, 50, 60, 70, 80, 90, and 100 $mV \cdot s^{-1}$.

Assemble of Zn-air battery

A Zn-air battery was assembled with a home-made cell in the size 4.2 × 4 × 4 cm^3. The Zn plate with working area 3.2 cm^2 acts as negative electrode. **Fe_3C/MoN** ink was casted on carbon paper equipped with air diffusion layer, which was employed as positive electrode. The working area of positive electrode is also 3.2 cm^2. The cell was filled with 25 mL mixed solution of 6 M KOH and 0.2 M $Zn(Ac)_2$. For comparison, the reference catalyst was prepared by mixing commercial Pt/C and RuO_2 with mass ratio of 1:1. No additional O_2 was introduced during battery testing

The specific capacitance of battery was calculated based on Eq. (5). In this equation, j and t are current density and discharge time. Δm_{Zn} represents the mass of Zn consumed.

$$C = jt/\Delta m_{Zn} \quad (5)$$

Assemble of flexible Zn-air battery

A flexible Zn-air battery was assembled in a sandwich-type configuration. The Fe_3C/MoN catalyst ink was cast onto carbon cloth and used as the air cathode, while Zn foil served as the anode. The effective working area of both electrodes was 3.2 cm^2.

A quasi-solid-state electrolyte, i.e., PAAK hydrogel saturated with 6 M KOH and 0.2 M $Zn(Ac)_2$, was introduced between the cathode and anode, followed by sealing the device with flexible packaging film. For comparison, the reference flexible Zn-air battery was fabricated using a mixed commercial Pt/C + RuO_2 catalyst (mass ratio = 1:1) as the air cathode under otherwise identical conditions. No additional O_2 was introduced during battery testing.

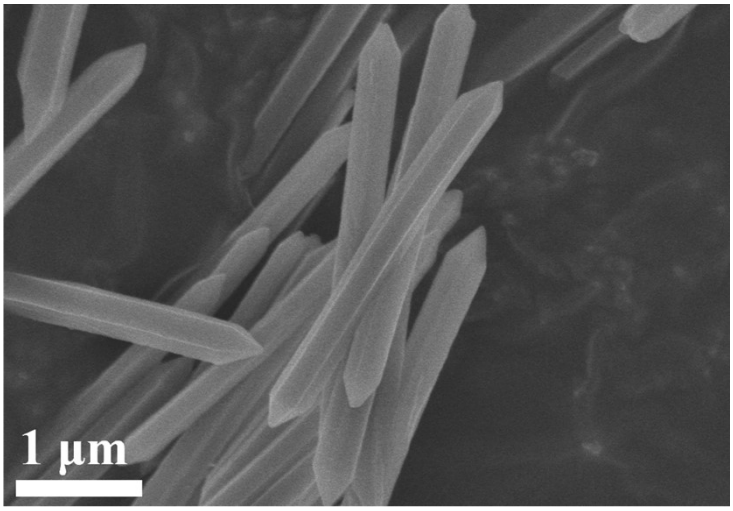

Fig. S1. SEM image of MIL-88A.

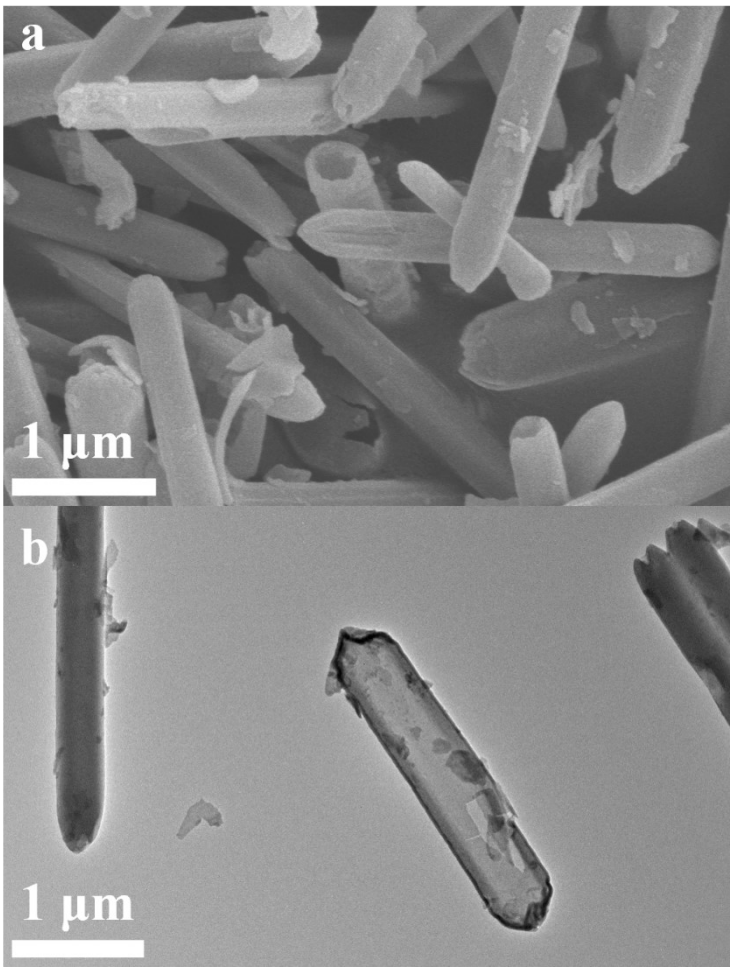

Fig. S2. (a) SEM and (b) TEM images of hollow Mo@MIL-88A intermediate.

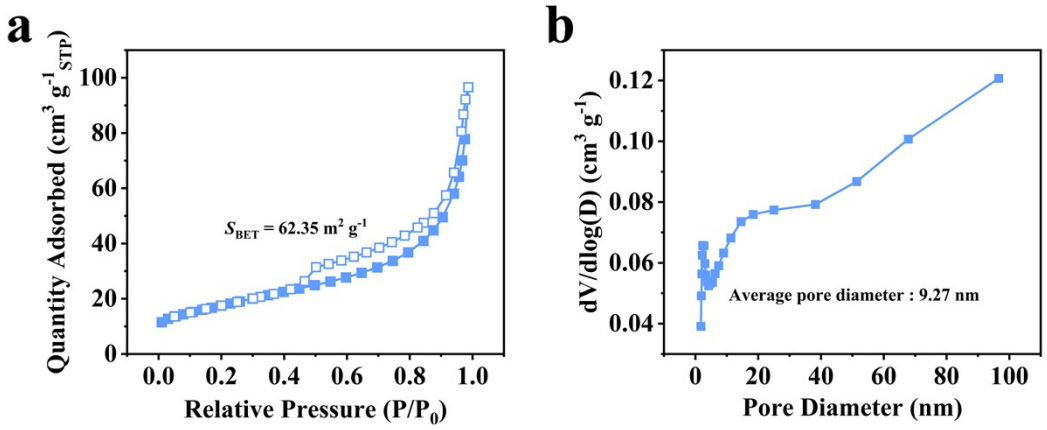

Fig. S3. (a) The N_2 adsorption–desorption isotherm and (b) pore size distribution curve of **Fe_3C/MoN**

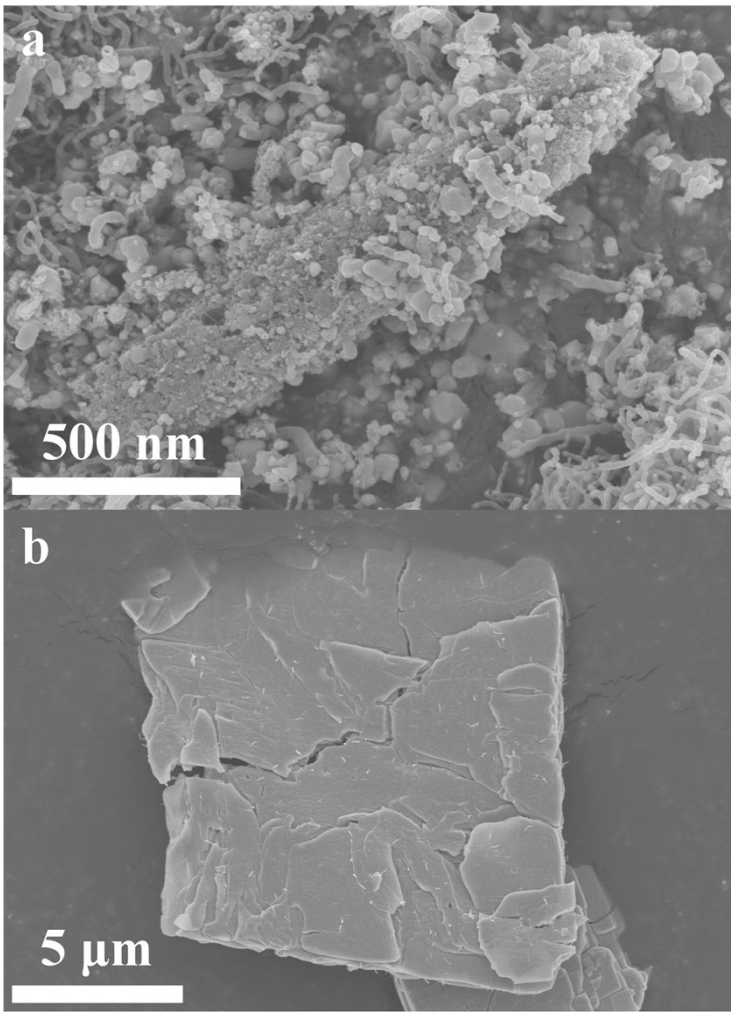

Fig. S4. SEM images of (a) Fe_3C and (b) MoN.

Note: Without the etching treatment, the MIL-88A precursor retains a solid rod-like structure and is prone to particle agglomeration during pyrolysis, yielding a dense, particulate rod-like Fe_3C rather than a hollow porous architecture. Meanwhile, owing to the bulky nature of the $NiMo_6$ polyoxometalate precursor, the derived MoN also lacks a well-defined morphology.

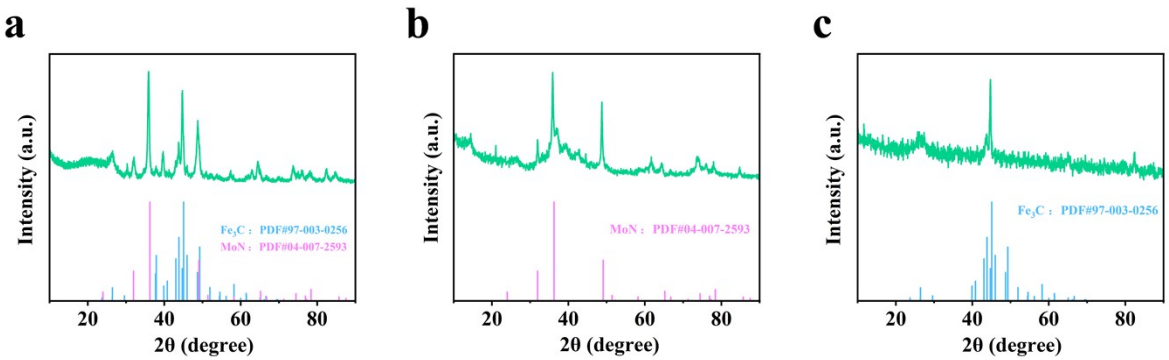

Fig. S5. XRD patterns of (a) **Fe_3C/MoN**, (b) MoN, and (c) Fe_3C.

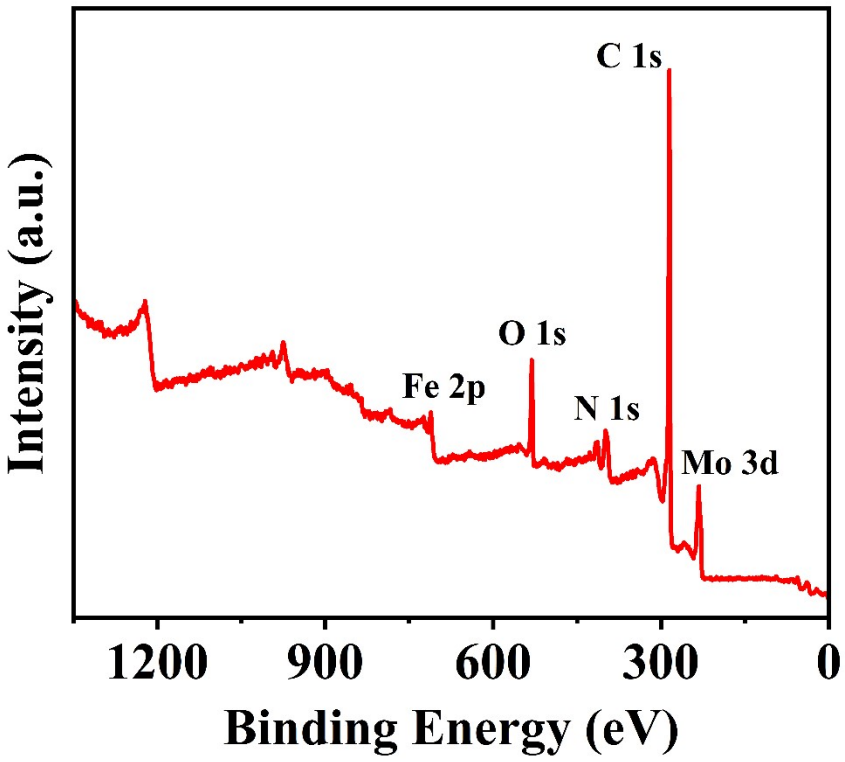

Fig. S6. XPS survey spectrum of **Fe_3C/MoN**.

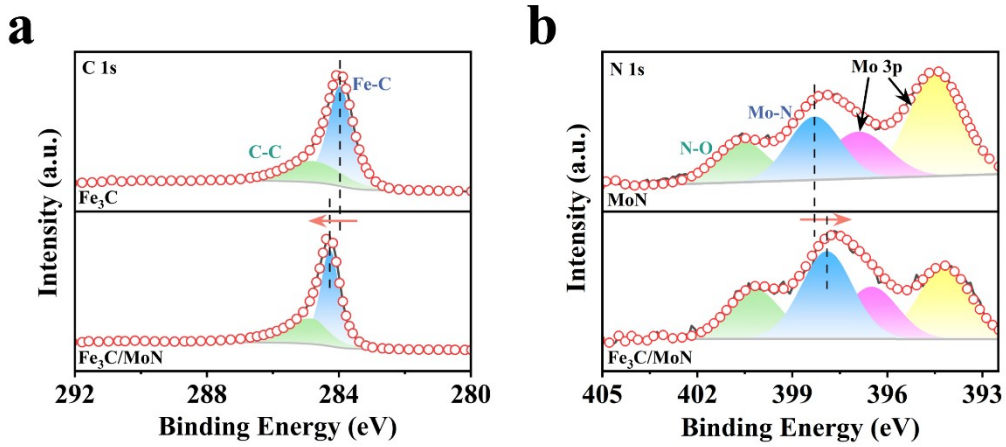

Fig. S7. (a) C 1s and (b) N 1s XPS spectra.

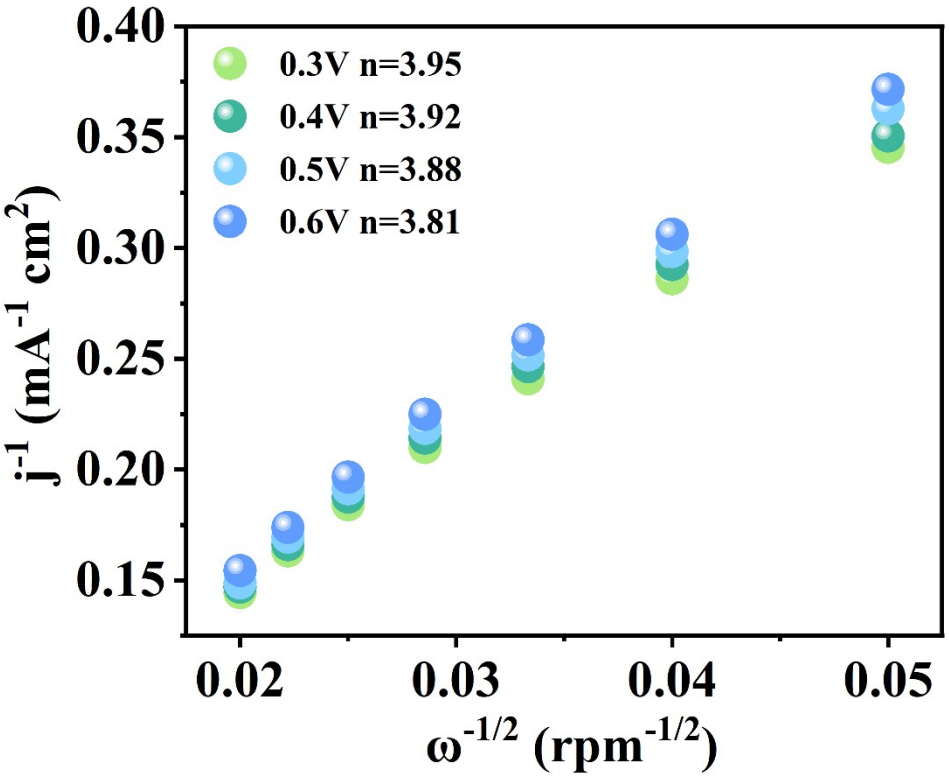

Fig. S8. K-L equation simulation of **Fe_3C/MoN**.

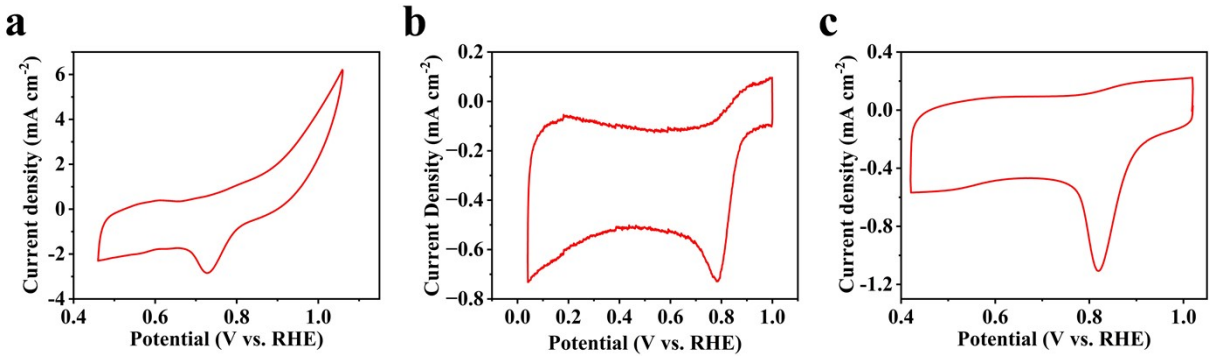

Fig. S9. CV curves of (a) Fe_3C, (b) MoN, and (c) commercial Pt/C in O_2-saturated 0.1M KOH electrolyte.

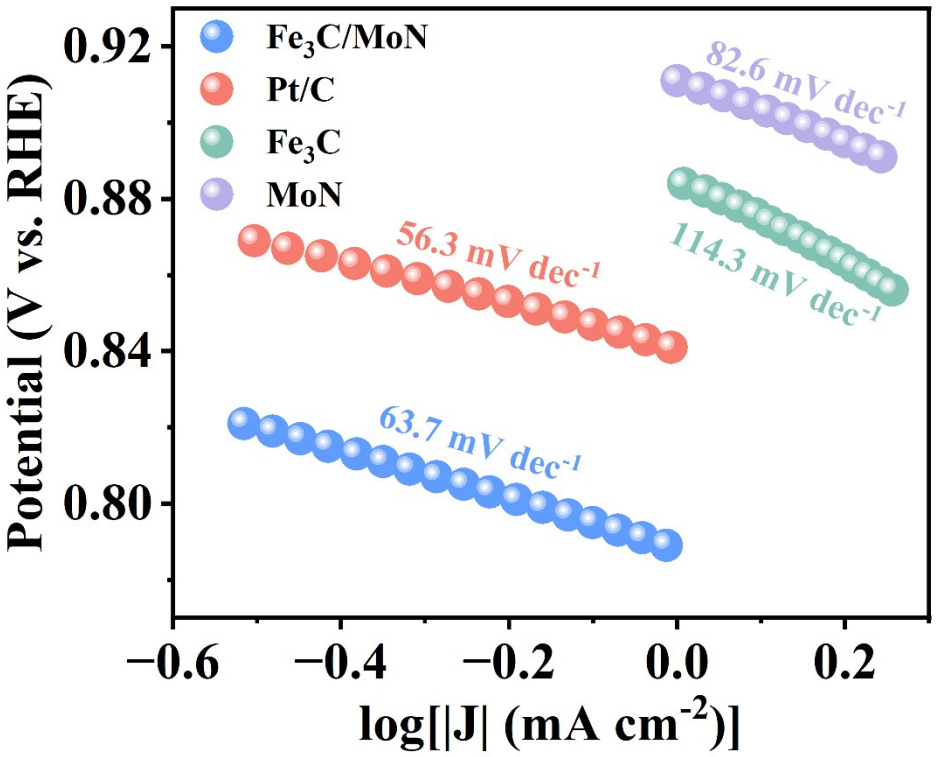

Fig. S10. ORR Tafel plots of **Fe_3C/MoN**, Fe_3C, MoN and Pt/C.

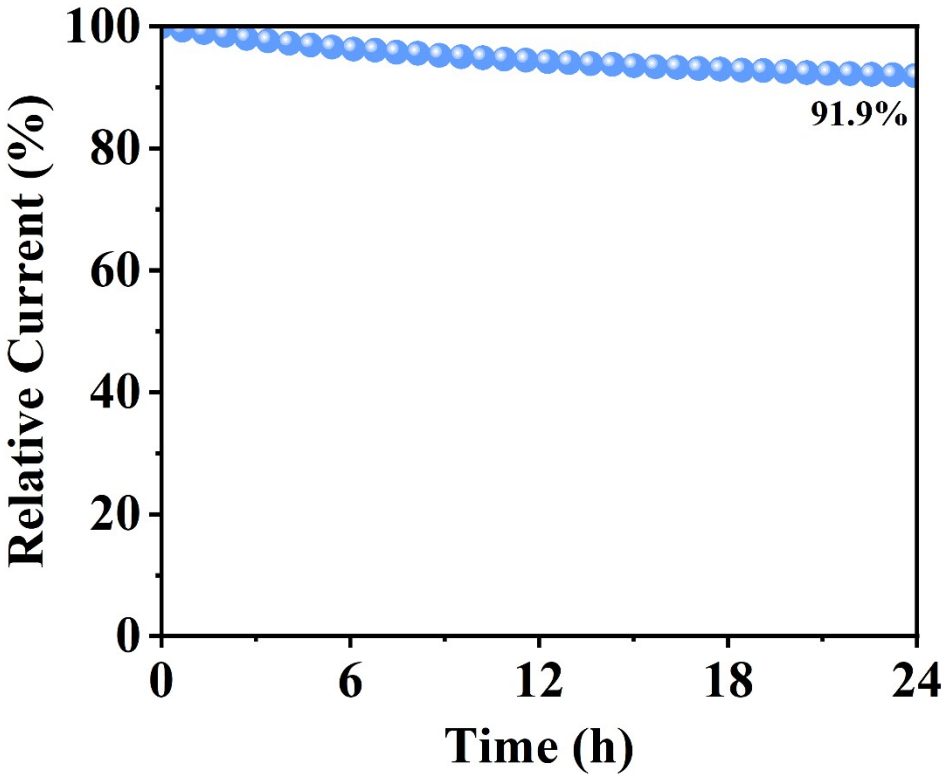

Fig. S11. Chronoamperometric (*i*-*t*) response of **Fe_3C/MoN** for ORR at $E_{1/2}$.

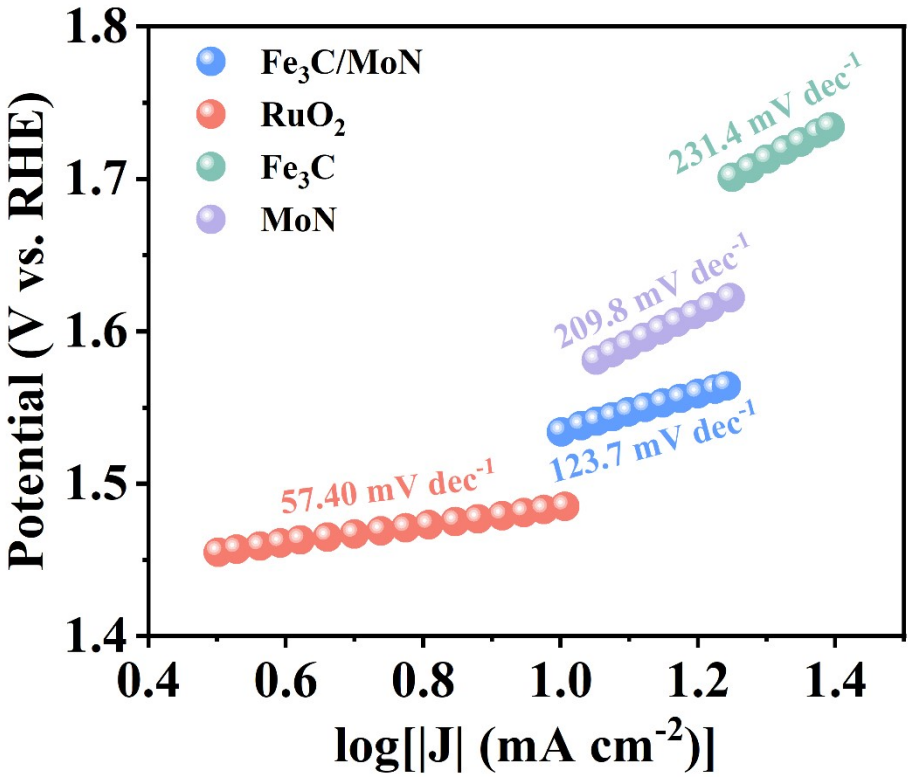

Fig. S12. OER Tafel plots of **Fe_3C/MoN**, Fe_3C, MoN and RuO_2.

.

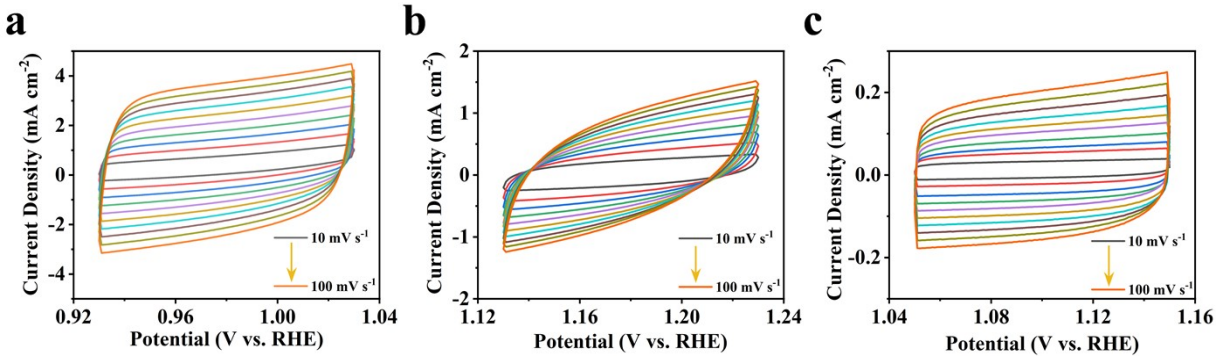

Fig. S13. CV curves of (a) **Fe_3C/MoN**, (b) Fe_3C, and (c) MoN at various scan rates.

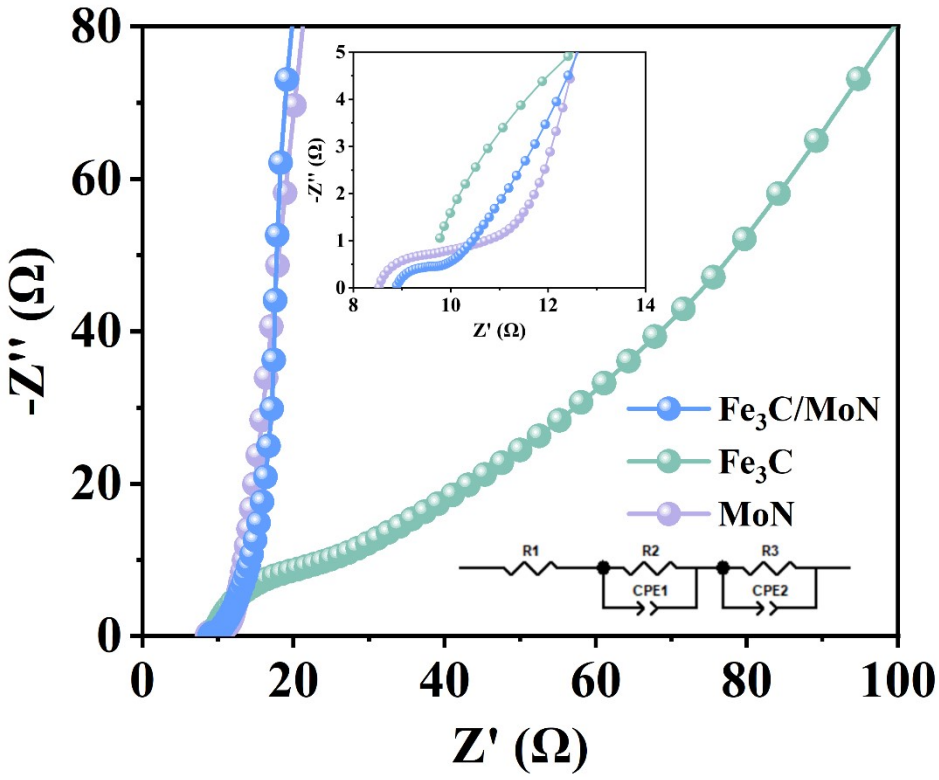

Fig. S14. Nyquist plots of **Fe_3C/MoN**, Fe_3C, and MoN.

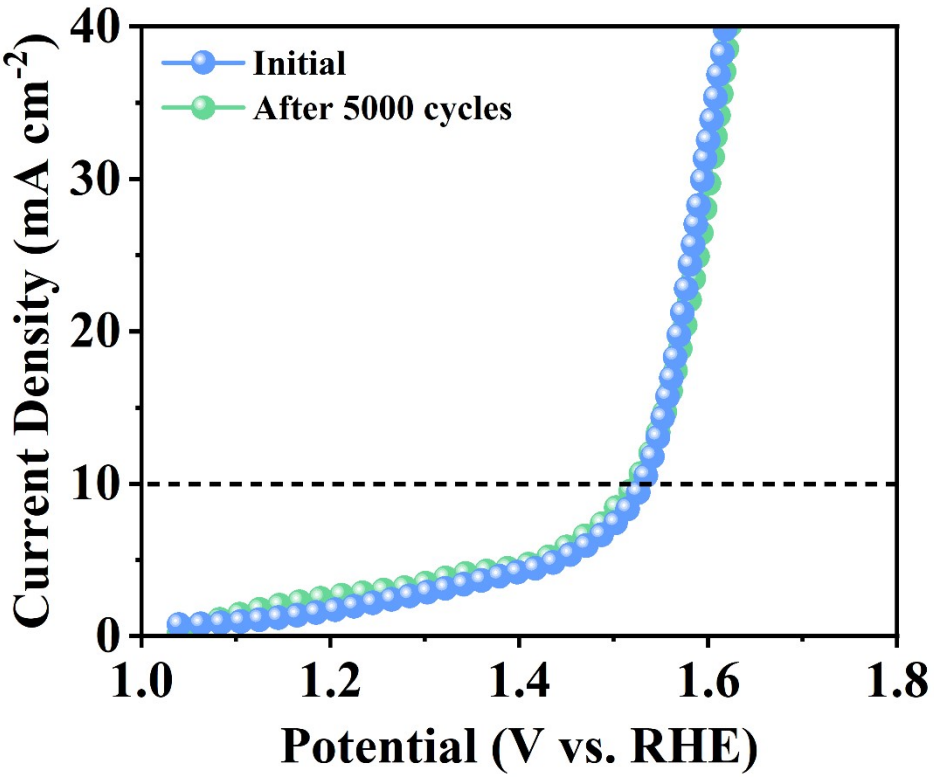

Fig. S15. OER LSV curves of **Fe_3C/MoN** before and after 5000 CV cycles.

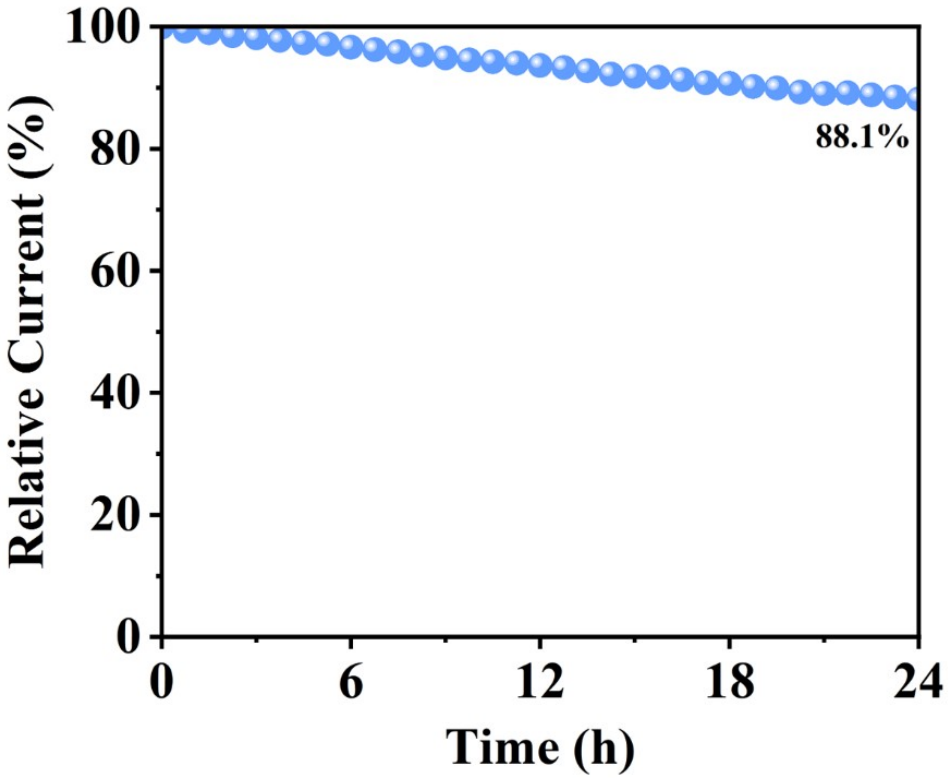

Fig. S16. *i-t* response of **Fe_3C/MoN** for OER at $E_{j=10}$.

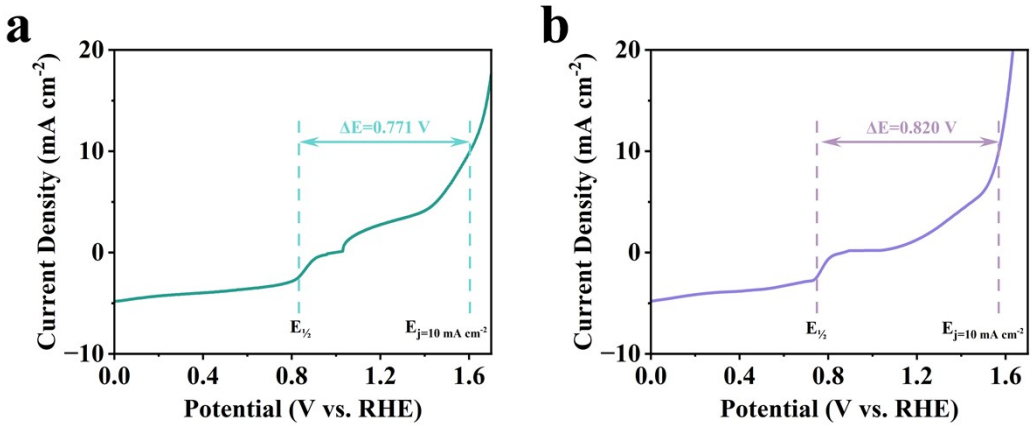

Fig. S17. Δ*E* values of (a) Fe_3C and (b) MoN.

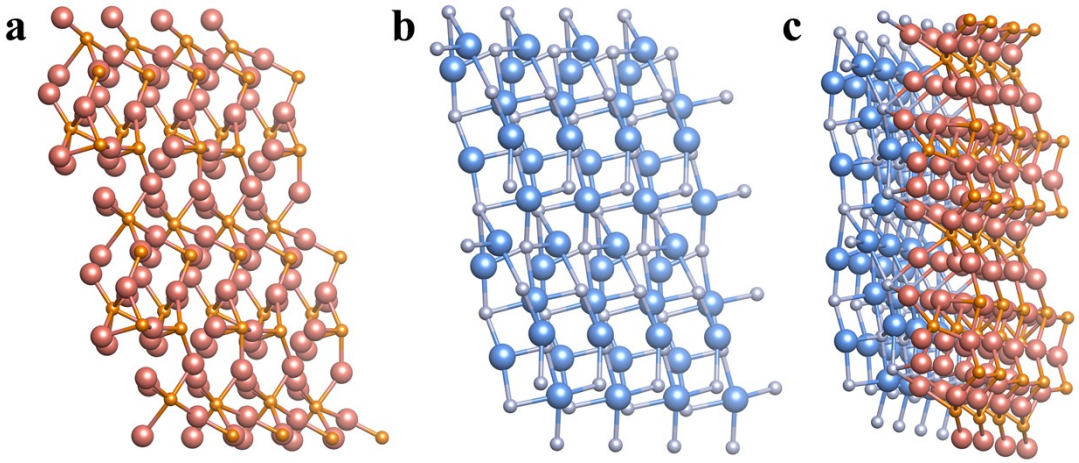

Fig. S18. Optimized structural models of (a) Fe_3C, (b) MoN, and (c) **Fe_3C/MoN.**

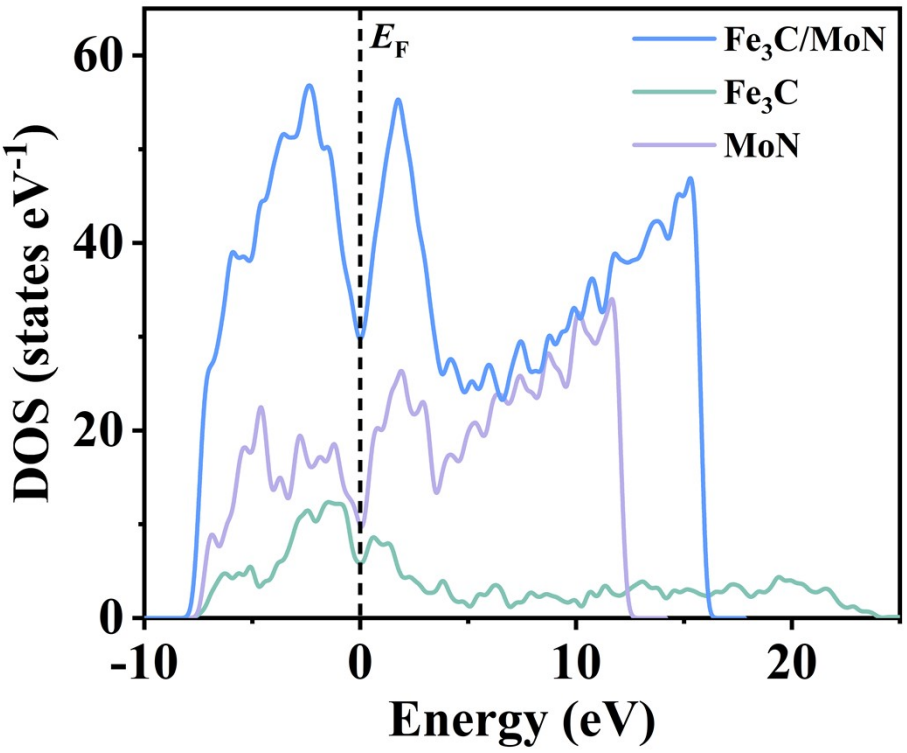

Fig. S19. Calculated DOS of Fe_3C, MoN, and **Fe_3C/MoN** with the Fermi level set to 0 eV.

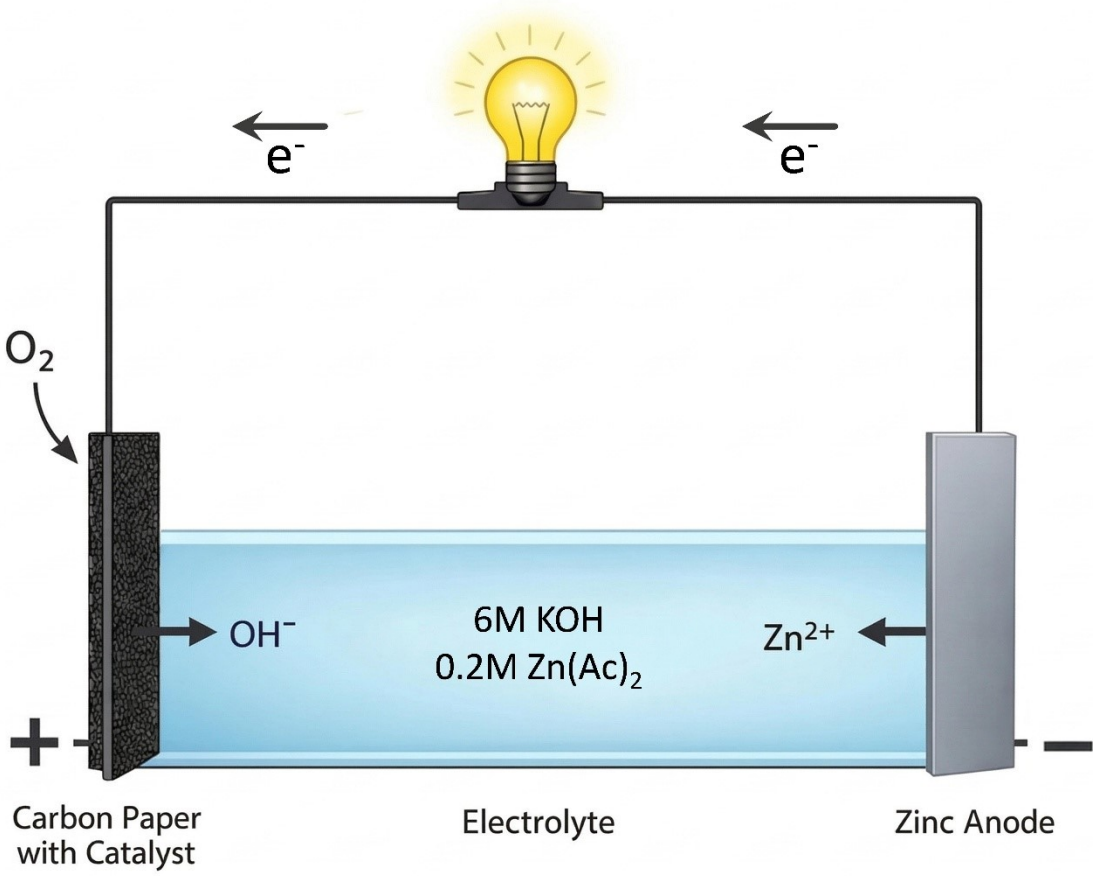

Fig. S20. Schematic illustration of the assembled ZAB.

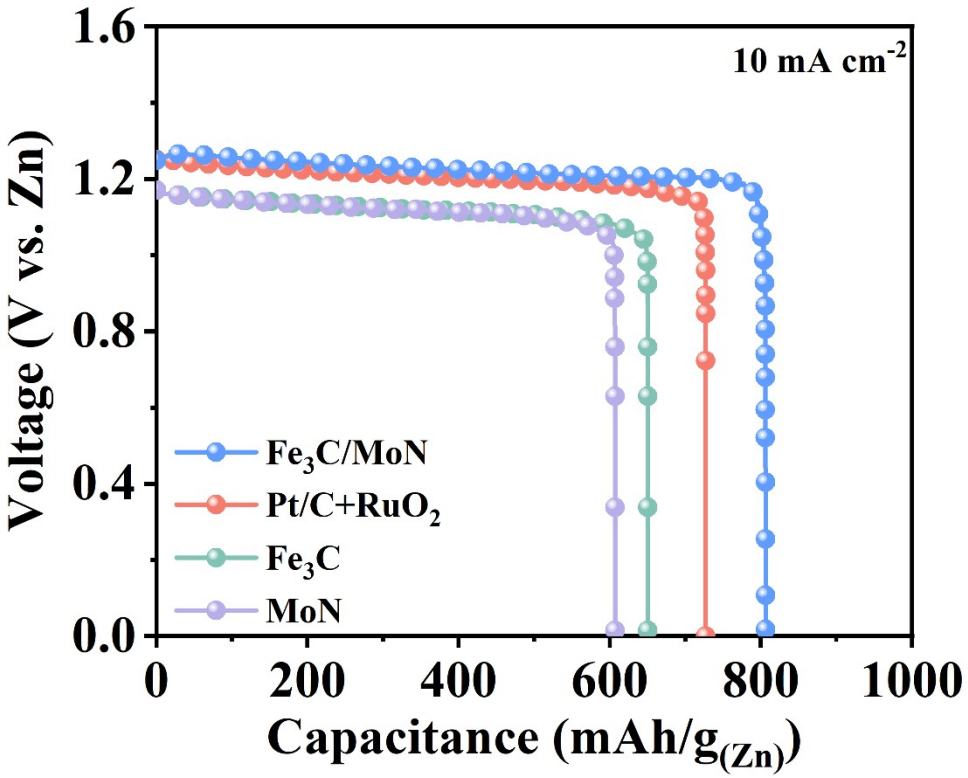

Fig. S21. Specific capacity of ZABs based on **Fe_3C/MoN**, Fe_3C, MoN and Pt/C + RuO_2 at 10 mA cm^{-2}.

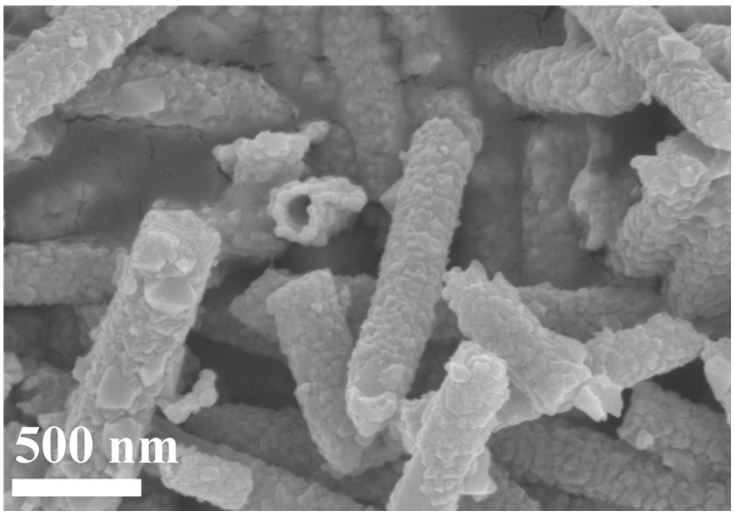

Fig. S22 SEM image of **Fe_3C/MoN** after 200 h ZAB GCD cycling.

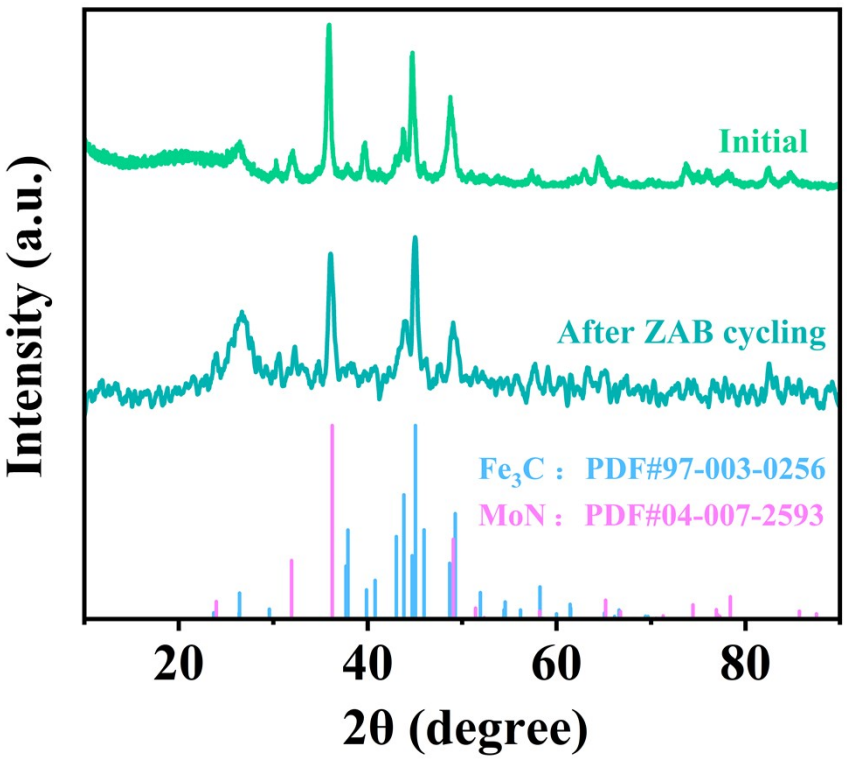

Fig. S23. XRD patterns of **Fe_3C/MoN** before and after 200 h ZAB GCD cycling.

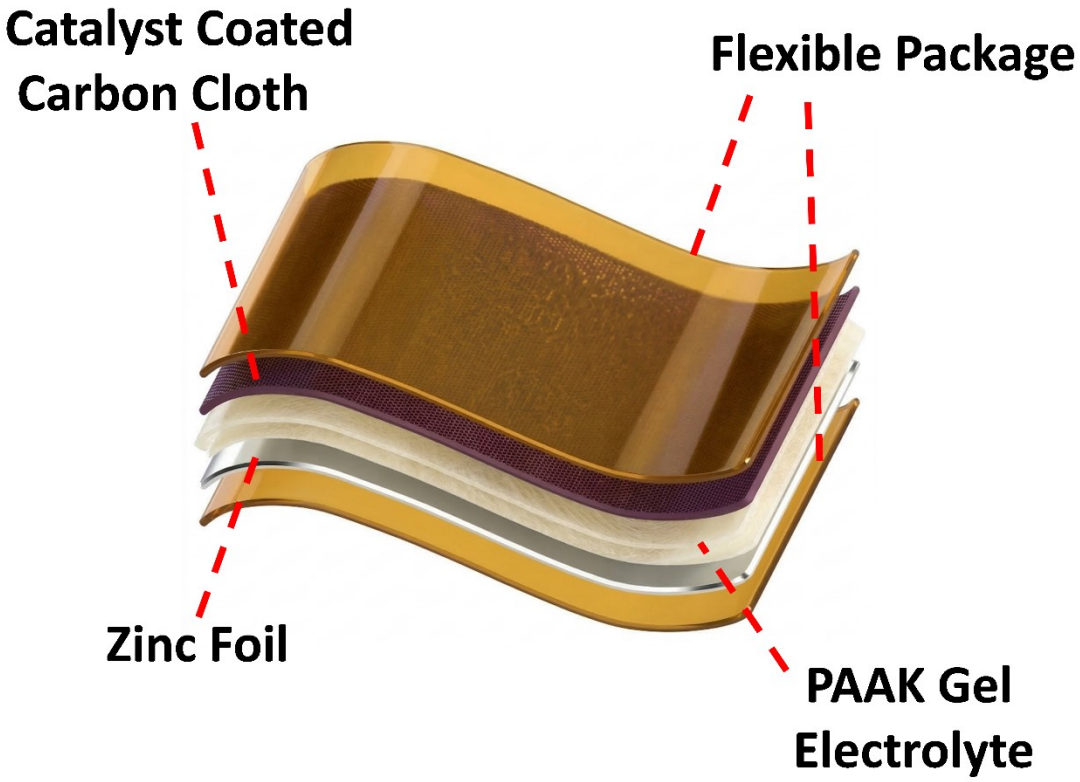

Fig. S24. Schematic illustration of the assembled FZAB.

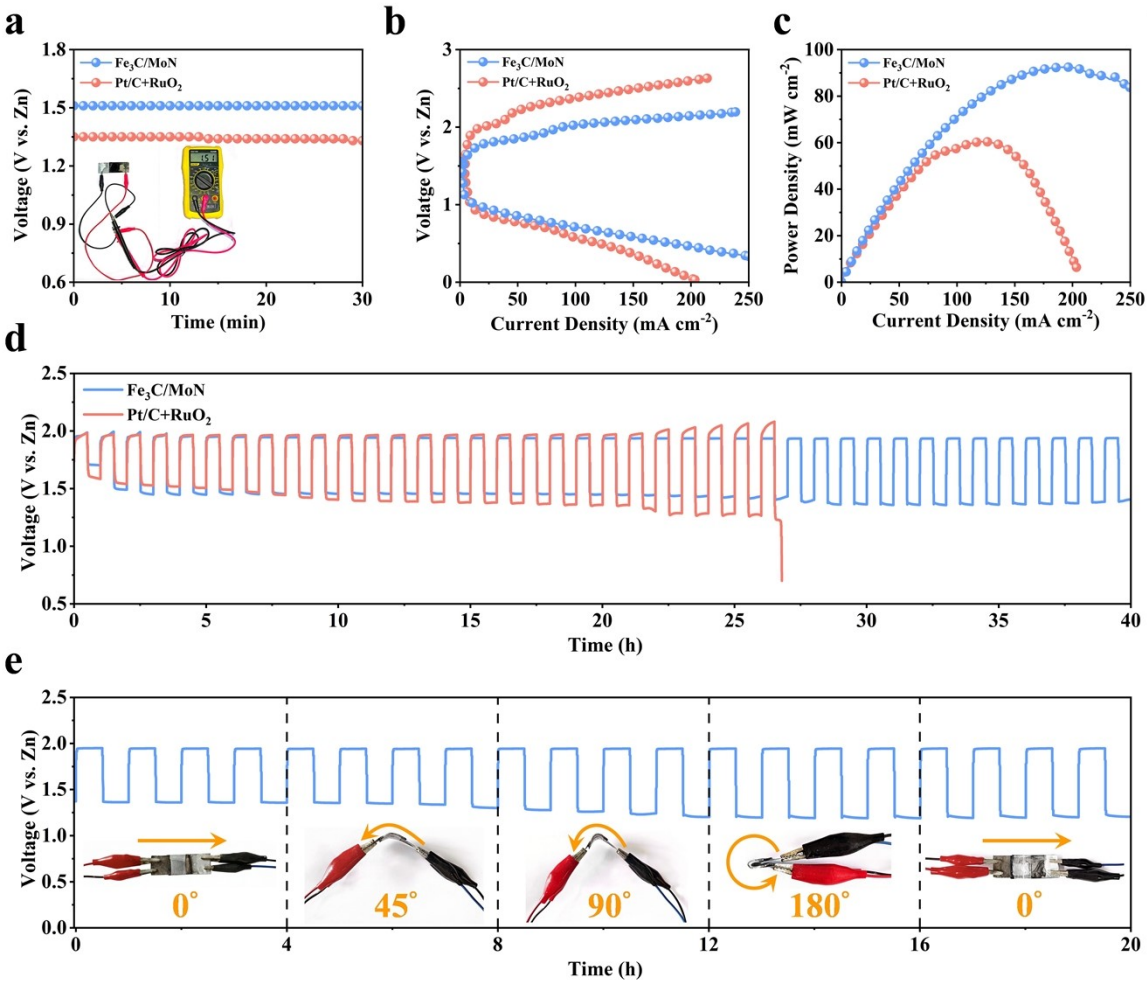

Fig. S25 (a) OCV curves, (b) polarization curves, (c) power density curves and (d) GCD cycling curves of **Fe_3C/MoN**- and Pt/C + RuO_2-based FZABs; (e) GCD cycling curve of **Fe_3C/MoN**-based FZAB under various bending angles.

Table S1. Surface elemental composition of **Fe_3C/MoN** determined by XPS survey spectra.

Element	Atomic percentage (at.%)
Fe	4.69
Mo	2.91
C	69.97
N	8.91
O	13.51

Note: The detected O species mainly arise from surface oxidation of **Fe_3C/MoN** and adsorbed oxygen species upon air exposure.

Table S2. Comparison of OER and ORR activities of **Fe_3C/MoN** with other Fe/Mo-based bifunctional electrocatalysts.

Electrocatalyst	$E_{1/2}$ (V)	η_{10} (mV)	ΔE (V)	Reference
Fe_3C/MoN	**0.854**	**305**	**0.681**	**This work**
FeCo/MoN@NCNTs	0.845	370	0.755	s1
FeMo/NCPs	0.85	390	0.77	s2
VN/Fe_3C@NCNT	0.845	337	0.722	s3
Fe_3C/MnO-NC	0.86	370	0.74	s4
Ce/Fe-NC/Fe_3C-P	0.87	389	0.749	s5
FeMn-NC	0.84	390	0.78	s6
Fe/Fe_3C@Fe-S-N-C	0.81	410	0.83	s7
(Fe_3C, Fe_3P)/NC	0.85	497	0.877	s8
Co-$Co_6Mo_6C_2$/CNFs	0.80	293	0.723	s9
Mo_2C/MoC/Co@CNTs	0.82	330	0.74	s10
Mo_2C-MoO_2/CMTs	0.80	320	0.75	s11
G-SHELL	0.72	320	0.83	s12
NC@MoS_2@Co-Fe	0.73	400	0.90	s13

References

[s1] Y. Zhang, W. Xue, Y. Ding, J. Chen and X. Xu, *Inorg. Chem. Commun.*, 2025, **177**, 114374.

[s2] J. Hu, S. Pang, S. Gao, H. Yu, N. Duan and S. Hu, *Compos. Part B Eng.*, 2025, **304**, 112695.

[s3] X. Li, J. Huang, D. Chu, L. Cao, X. Zhang, Q. Chen, K. Kajiyoshi, Y. Liu and L. Feng, *Energy*, 2025, **319**, 135045.

[s4] J. Zhong, Q. Xu, R. Li and D. Yuan, *Appl. Catal. B: Environ. Energy*, 2025, **361**, 124615.

[s5] L. Wang, X. Liu, K. Su, W. Liu, F. Niu, X. Li, H. Yue, H. Dong, S. Yang and Y. Yin, *ACS Appl. Nano Mater.*, 2024, **7**, 22855–22864.

[s6] R. Li, D. Zhu, L. Peng, Y. Yang, K. Qi and D. Yuan, *J. Energy Storage*, 2025, **131**, 117513.

[s7] T. Luo, W. Huan, J. Liang, P. Wang, T. Liu, Z. Long, J. Li, J. Shuai, P. Zhu, X. Zhao and S. Liu, *J. Energy Storage*, 2026, **151**, 120522.

[s8] S. Xiao, P. Zheng, L. Han, Q. Luo, S. Long, X. Zeng, Y. Zhang and P. Dong, *ACS Appl. Energy Mater.*, 2024, **8**, 529–537.

[s9] S. Xu, Y. Feng, J. Bai, X. Sun and C. Li, *J. Alloys Compd.*, 2024, **1005**, 176151.

[s10] C. Xu, J. Zuo, J. Wang and Z. Chen, *J. Power Sources*, 2024, **595**, 234063.

[s11] X. Zhang, X. Zhu, X. Liu, X. Liu and S. Alwarappan, *Small*, 2025, **21**, e2502395.

[s12] D. W. Kim, J. Kim, J. H. Choi, D. H. Jung and J. K. Kang, *Adv. Sci.*, 2024, **11**, e2408869.

[s13] X. Shang, Q. Shen, Y. Xiong, Z. Jiang, C. Qin, X. Tian, X. Yang and Z.-J. Jiang, *J. Alloys Compd.*, 2022, **916**, 165482.